The 20th Cambridge Workshop on Cool Stars, Stellar Systems, and the Sun
Edited by S. J. Wolk

Multiple populations in young clusters detected by Gaia.

Veronica Roccatagliata[1]

[1] INAF/Osservatorio Astrofisico di Arcetri - Largo E. Fermi 5, 50125, Firenze - Italy ; veronica.roccatagliata@inaf.it

Abstract

The second release of *Gaia* is revolutionizing the study of star formation and young clusters. In this talk I discussed the potential in detecting multiple populations in young clusters, and the importance of a membership well defined as a starting point. I presented, as an example, the results on the multiple population of one of the closest low-mass star forming region, the Chamaeloen I. Using the *Gaia* data we found the region to be at slightly higher distance than previously thought. We confirmed the presence of two populations with a peculiar spatial distribution, which might be influenced by the filamentary molecular cloud present in the region. Presenting the method applied to find kinematically the multiple populations, I discussed the effect on the results of taking into account the correlations between parallaxes and proper motions. I finally presented the impact of the refined distance of young stars and clusters using the *Gaia* data on other fields of star formation, e.g. the study of the evolution of protoplanetary disks and the disk structure.

1 Introduction

Gaia is revolutionising the different fields of stellar astrophysics providing a three-dimensional map of the Milky Way. This has a fundamental impact also in the field of stars and cluster formation. On one side several studies are analyizing large scale regions in combination with photometric surveys, as the Vela OB2 (e.g. Armstrong *et al.* (2018); Cantat-Gaudin *et al.* (2018)), on the other side or looking for new members in nearby associations (e,g. Gagné & Faherty (2018)) or discover new nearby associations (e.g. Gagné *et al.* (2018)).
Another approach is to concentrate a study on a single region to investigate whether multiple stellar populations are present in the each star forming region, and if different star formation episodes took place in the region. This is much more efficient when it uses, as starting point, a sample of sure members of a region previously identified by other studies, from which compute the mean parallax and proper motions of the region.
An example of such approach is represented by the study of one of the closest low-mass star forming regions, Chamaeleon I. Thanks to its proximity, it is possible to study all the key processes taking place during the star formation process, from the filaments to the structure of different classes of protoplanetary disks, as well as the dynamics of the young cluster.
The distance of Chamaeleon I commonly adopted in the literature is 160 ± 15 pc Whittet *et al.* (1997). This value comes from the combination of the value of 135 - 165 pc obtained from the extinction and the weighted average of Hipparcos distances for three cluster members (HD 97300, HD 97048 and CR Cha), is 175^{+20}_{-16} pc Perryman *et al.* (1997). Recentely, using the Tycho-Gaia Astrometric Solution catalog from the first release of the *Gaia* data, Voirin *et al.* (2018) revised the Hipparcos distance of Chamaeleon I to 179^{+11+11}_{-10-10} pc.
In the last fifteen years several studies aimed at the definition of the stellar content of Chamaeleon I (e.g. Feigelson & Lawson (2004); Stelzer *et al.* (2004); Comerón *et al.* (2004)).
A fundamental finding was that Chamaeleon I has two populations spatially separated with different ages: 5-6 Myr for the northern and 3-4 Myr for the southern sub-cluster, respectively (Luhman (2007)). Sacco *et al.* (2017) confirmed kinematically the presence of the two sub-clusters, with a shift in velocity of about 1 km/s. Moreover, the velocity dispersion of the stellar population was found to be more than two times higher than the dispersion of the pre-stellar cores derived from the sub-millimeter observations.
The *Gaia* DR2 astrometry (Gaia Collaboration *et al.* (2018); Lindegren *et al.* (2018)) recently released clearly offers an unique opportunity to give fundamental insides on the still open debate on the general distance of Chamaeleon I, as well as to look for indications of the multiple population previously found.

In this talk I mainly presented new results published in a letter (Roccatagliata, V. *et al.* (2018)) right accepted during the conference. We analyzed the new accurate measurements of parallaxes and proper motions of the cluster members spectroscopically identified by previous works. This approach aims at the characterization of the known populations of Chamaeleon I, rather than discover possible new members of the region.

I discussed also the impact of the refined distance of young stars and clusters on other fields of star formation, e.g. the study of the evolution of protoplanetary disks and the disk structure.

2 Data

A catalog of 244 optical members has been compiled combining the observations of Luhman (2007) and Sacco *et al.* (2017). From this initial catalog, 206 sources are present in the *Gaia* DR2 archive, but for any further analysis we consider only the 140 with an excess source noise less than 1, as suggested e.g. by Lindegren *et al.* (2018).
The distribution of the parallaxes of the cluster members is

shown in Figure 1, with highlighted the distance commonly adopted in the literature for Chamaeleon I.
Assuming that all the cluster members belong to the same population, the resulting median parallax is 5.248±0.187 mas, where the associated error is computed as the median absolute deviation (MAD). The distance was then computed by inverting the parallax, since the relative error of the parallax is lower than 10% (Luri *et al.* (2018); Bailer-Jones (2015)). The distance of Chamaeleon I is, hence, $\mathbf{190.5}^{+7.1+3.8}_{-6.5-3.5}$ **pc**, which takes into account a conservative systematic error of 0.1 mas, as discussed by Luri *et al.* (2018). This distance is larger than previously assumed in the literature Whittet *et al.* (1997), while being marginally consistent with the Hipparcos distance from three members only, as well as the TGAS results obtained by Voirin *et al.* (2018).

3 Analysis

The spatial distribution of the cluster members (after a 3-sigma clipping on the initial sample) plotted as a function of the parallaxes and proper motions reveals that the two subclusters spatially identified by Luhman (2007) can be clearly distinguished also in parallax and kinematically.
The quantitative analysis of the *Gaia* data proceeded in two steps:

1. use a statistical method to confirm the existence of the northern and southern sub-clusters separated in parallax and kinematics,

2. analyse the new *Gaia* parallax and proper motions taking into account the covariance between the data.

The northern and southern regions have been selected using the criterium of Luhman (2007) based on their declinations (higher or lower than -77°, respectively).
The two-sample *Kolmogorov-Smirnov test* in parallaxes and proper motions gave probabilities that the two samples belong to the same parent population of $2.39 \cdot 10^{-12}$, $8.0 \cdot 10^{-14}$ and $1.84 \cdot 10^{-11}$ in parallax, proper motion in α and δ, respectively. This confirms statistically that the two clusters are spatially separated in parallax and kinematically separated in proper motions.
During my talk I highlighted the importance in the *Gaia* studies of clusters of taking into account all the covariances between quantities as done by Luri *et al.* (2018). Without this caution, it is possible to introduce spurious signals in the data (e.g. Brown *et al.* (1997)).
The *Gaia* catalog gives all the uncertainties on the astrometric data in the full covariance matrix for each source. The diagonal elements are the standard uncertainties of the astrometric parameters, while the off-diagonal elements are the covariances (which are the correlations between the uncertainties). For all these reasons we decided to model the distribution of the three astrometric parameters (π_i, $\mu_{\alpha,i}$, and $\mu_{\delta,i}$) with a 3D multivariate gaussians (as in Equations 6-10 in Lindegren *et al.* (2000)). The likelihood function for each star of each population is given by

$$L_{N/S,i} = \frac{\exp -\frac{1}{2}(a_i - a_0)' \, C_i^{-1} \, (a_i - a_0)}{(2\pi)^{3/2} \, |C_i|^{1/2}} \qquad (1)$$

where

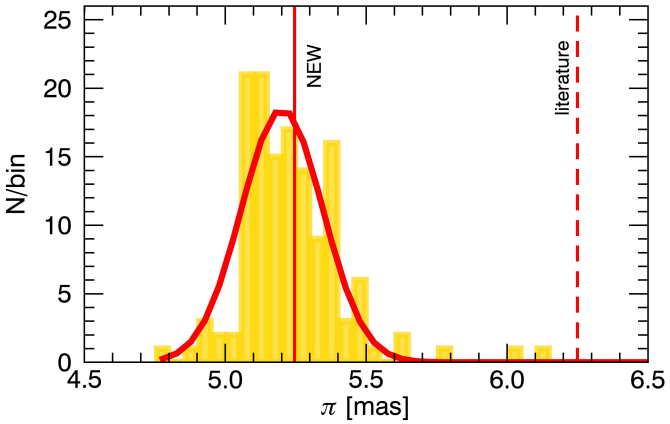

Figure 1: Histogram of the parallaxes of the Chamaeleon I members, with highlighted the position of the median parallax and the parallax commonly adopted from the literature (adapted from Fig.1 in Roccatagliata, V. *et al.* (2018)).

- $(a_i - a_0)'$ is the transpose of the vector

$$a_i - a_0 = \begin{matrix} \pi_i - \pi_0 \\ \mu_{\alpha,i} - \mu_{\alpha,0} \\ \mu_{\delta,i} - \mu_{\delta,0} \end{matrix} \qquad (2)$$

  where π_0, $\mu_{\alpha,0}$, $\mu_{\delta,0}$ are the mean values of the cluster.

- C_i is the covariance matrix, $|C_i|$ its determinant. Following Lindegren *et al.* (2000), the covariance matrix C_i of Equation 1 corresponds to

$$C_i = \begin{matrix} C_{i,11} & C_{i,12} & C_{i,13} \\ C_{i,21} & C_{i,22} & C_{i,23} \\ C_{i,31} & C_{i,32} & C_{i,33} \end{matrix} \qquad (3)$$

  and each term of the matrix to

$$\begin{aligned} C_{i,11} &= \sigma^2_{\pi,i} + \sigma^2_{\pi,0} \\ C_{i,22} &= \sigma^2_{\mu_{\alpha,i}} + \sigma^2_{\mu_{\alpha,0}} \\ C_{i,33} &= \sigma^2_{\mu_{\delta,i}} + \sigma^2_{\mu_{\delta,0}} \\ C_{i,12} &= C_{i,21} = \sigma_{\pi,i} \cdot \sigma_{\mu_{\alpha,i}} \cdot \rho\,(\pi, \mu_\alpha) \\ C_{i,13} &= C_{i,31} = \sigma_{\pi,i} \cdot \sigma_{\mu_{\delta,i}} \cdot \rho\,(\pi, \mu_\delta) \\ C_{i,23} &= C_{i,32} = \sigma_{\mu_{\alpha,i}} \cdot \sigma_{\mu_{\delta,i}} \cdot \rho\,(\mu_\alpha, \mu_\delta) \end{aligned} \qquad (4)$$

  where $\rho\,(\pi, \mu_\alpha)$, $\rho\,(\pi, \mu_\delta)$, $\rho\,(\mu_\alpha, \mu_\alpha)$ are the correlation coefficients[1], $\sigma_{\pi,i}$, $\sigma_{\mu_{\alpha,i}}$ and $\sigma_{\mu_{\delta,i}}$ are the errors associated to each measurement[2], while $\sigma_{\pi,0}$, $\sigma_{\mu_{\alpha,0}}$ and $\sigma_{\mu_{\delta,0}}$ are the intrinsic dispersions of π, μ_α and μ_δ obtained from the Maximum Likelihood Estimation of the probability given in Eqs. 1.

Our calculations including two populations make use of the maximum likelihood approach presented in Jeffries *et al.* (2014) and Franciosini *et al.* (2018). The probability for each star of belonging to either the sub-cluster A or B is computed as

$$P_{N,i} = f_N \frac{L_{N,i}}{L_i} \quad P_{S,i} = (1 - f_N) \frac{L_{S,i}}{L_i} \quad , \qquad (5)$$

[1] from the *Gaia* archive

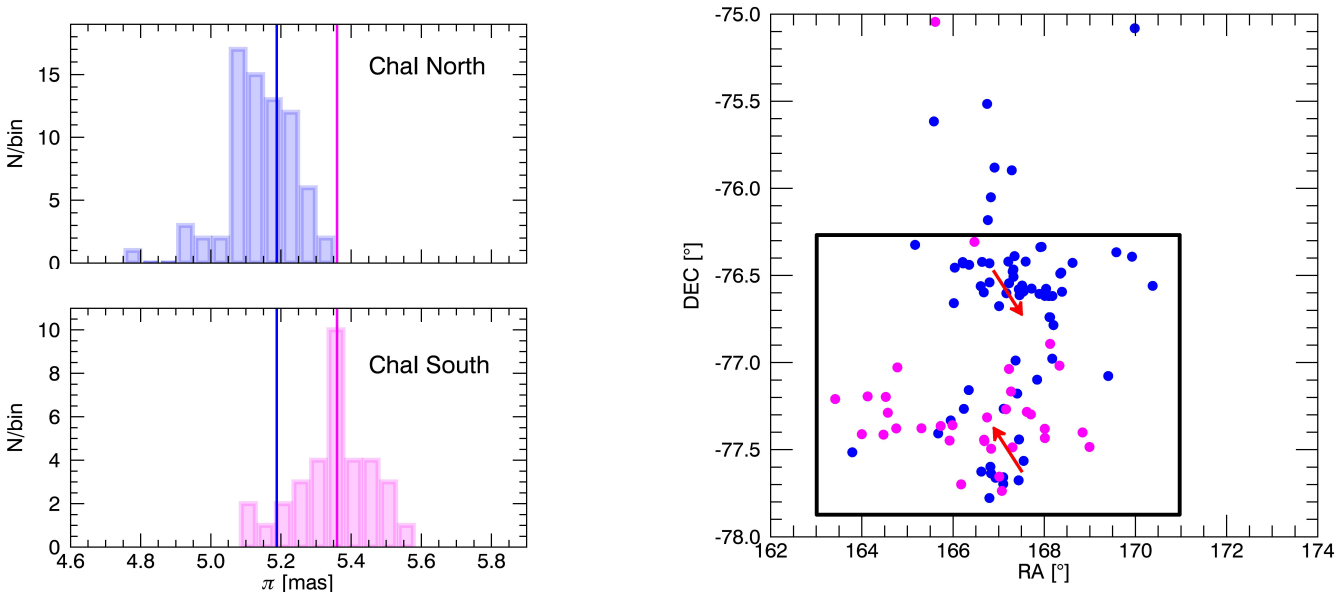

Figure 2: *Left:* Histograms of the parallax distributions of the most probable members (P≥80%) of the northern (in blue) and southern (in magenta) sub-clusters. The vertical lines represent the MLE parallaxes for both clusters. *Right:* Spatial distribution of the northern (blue symbols) and the southern (magenta symbols) sub-cluster. The red arrows represent the differential proper motions in α and δ with respect to a mean proper motion between the northern and southern cluster. The black box represents the region covered by Figure 3.

The total likelihood of the double population is therefore given by:

$$L_i = f_N\, L_{N,i} \,+\, (1 - f_N)\, L_{S,i} \qquad (6)$$

where L_N and L_S are the likelihoods given in Equation 1 for the northern and southern sub-clusters, f_N is the fraction of stars that belongs to the north component, and $f_S = (1 - f_N)$ is the fraction of southern stars.
This is a reliable assumption for this region since our membership is based on different accurate studies where two populations have been already detected.

4 Results and Discussion

From the initial members from Luhman (2007), we found 140 sources with a reliable parallax and proper motions. 107 stars had a probability higher than 80% to belong to one of the two sub-clusters. Additional details can be found in Roccatagliata, V. *et al.* (2018).
The uncertainties in parallax and proper motions considered in the analysis include only the errors provided in the *Gaia* DR2 archive. [2]

In Figure 2 we show the histograms of the parallax distribution of the 73 most probable northern members, and the 34 southern members, with highlighted the parallaxes of the two sub-clusters computed from the maximum likelihood estimation (MLE). Inverting the parallaxes, we derive the distances of the two sub-clusters:

$$\mathbf{d_N = 192.7^{+0.4}_{-0.4}\ pc} \qquad \mathbf{d_S = 186.5^{+0.7}_{-0.7}\ pc}.$$

In the right panel of Figure 2 the spatial distribution of the two sub-clusters shows that the projected distance between the centers of both clusters along the line of sight is of the same order as their projected separation in the plane of the sky and as their spatial extent. This supports the hypothesis that they both belong to the same physical entity, and it is not only a chance alignment along the line of sight. We see that the southern cluster has a compact structure, while the northern one, which corresponds to the more distant one, is spatially more elongated and it extends in the direction of the southern cluster.

This may reflect the influence of the 3D extension of the main filamentary structure present in the region, which extends in the north-south direction. This filament was mapped in $C^{18}O$ by Haikala *et al.* (2005) and in the far-infrared by *Herschel* (Figure 3).

4.1 The age of Chamaeleon I

Taking into account the most probable members (with P>80%) of Chamaeleon I, we investigate whether an age difference is present between the two sub-clusters. In order to minimize the effects due to infrared excesses caused by the presence of protoplanetary discs, we use the $\log(T_{eff})$-M_J diagram. The absolute J magnitude of each source has been derived by adopting the mean distance module for the northern and southern sub-clusters and correcting for A_J Luhman (from 2007). The overplotted isochrones are the Z=0.013 models from Tognelli *et al.* (2011) [3].
All the sources have ages lower than 5 Myr. In particular, apart for few sources, most of the members are younger than 3 Myr. In contrast to the different ages for the two populations (5-6 Myr for the northern one and 3-4 Myr for the southern one) found by Luhman (2007) found, we do not

[2] Luri *et al.* (2018) suggested to discuss at the end of the analysis a possible influence on the scientific results of a systematic error not larger than 0.1 mas in parallax and 0.1 mas/yr for proper motions.

[3] `https://www.astro.ex.ac.uk/people/timn/tau-squared/pisa_details.html`

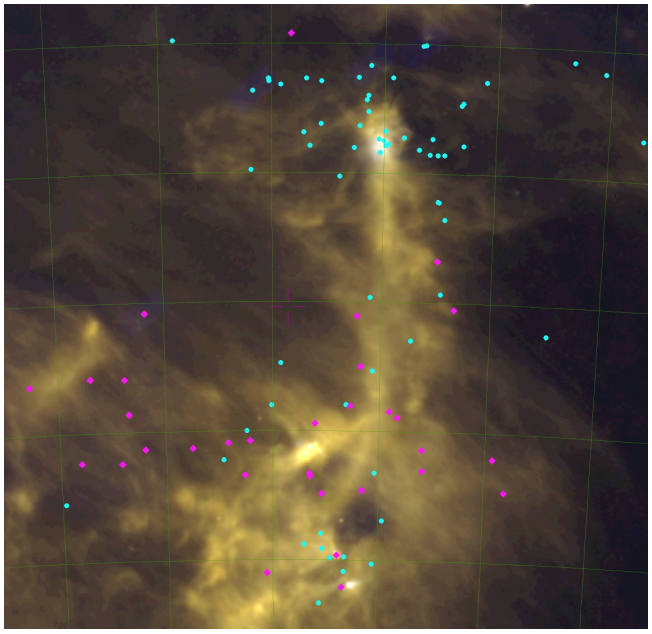

Figure 3: *Herschel* composite image in the far-infrared of the region highlighted by the black square in Figure 2. The symbols represent the 2 cluster members (color code as in in Figure 2).

find any evidence of an age difference between the two sub-clusters.
This can be explained with the combination of two effects: on one side, Luhman (2007) used the same distance to all sources adopting a smaller value than what we find here; on the other side, his selection of the two sub-clusters was based only on the spatial distribution, while in our case we take into account also their different parallaxes and kinematic properties.

4.2 Kinematics properties of the North and South sub-clusters

Under the assumption of an isotropic distribution in a star cluster, we derived the velocity dispersion from the proper motion dispersion obtaining $\sigma_{r,N} = 0.681 \pm 0.057$ km/s and $\sigma_{r,S} = 0.727 \pm 0.134$ km/s, where the uncertainties are computed from the error propagation. The velocity dispersions are consistent, within 2 σ, with the results of Sacco *et al.* (2017).
Given that the northern cluster is in the background, and it is more redshifted than the closer southern sub-cluster, we conclude that the two clusters are moving away from each other.
The two arrows in Figure 2 represent the differential proper motions of the two sub-clusters with respect to a reference system centered on the cluster. Combining this result with the differential radial velocity measured by Sacco *et al.* (2017), we can draw the following conclusions:

- the two sub-clusters are not merging
- the sub-clusters have a non-zero angular momentum
- the sub-clusters might rotate

In young high-mass clusters rotation has been theoretically predicted by Mapelli (2017), and it has been observed e.g. in the high-mass star forming region R136 in the Large Magellanic Cloud Hénault-Brunet *et al.* (2012). However, in simulations with similar total mass to low-mass environments, such as Chamaeleon I, Mapelli (2017) did not find a clear signature of rotation as in high-mass environments.

5 Impact of *Gaia* on other fields related to young stars and clusters

The 3D view of star forming regions has a fundamental impact on fundamental studies on the disk dissipation as a function of time. These studies started in near-infrared with Haisch *et al.* (2001) who found a drastic decrease with time of the excess sources to the total number of cluster members. These studies exploded with the results from *Spitzer* on low-mass star forming regions (e.g. Hernández *et al.* (2007); Sicilia-Aguilar *et al.* (2006)). The study of the influence on disk dissipation was also done analyzing the effect of high-mass stars in the disk fractions (e.g. IC 1795 in Roccatagliata *et al.* (2011)). The *Gaia* data will allow
- the spatial and kinematical definition of the cluster membership;
- the discover or confirmation of multiple populations;
- a 3D view on the sky of the clusters;
- to compute linear sizes and distances within the cluster.

We are now also in the ALMA era when an increasing number of protoplanetary disks have been resolved, revealing a gallery of rings (e.g. Andrews *et al.* (2016); Fedele *et al.* (2017, 2018)), cavities (e.g. Zhang *et al.* (2014)), arcs (e.g. van der Marel *et al.* (2013)) or spirals (e.g. Pérez *et al.* (2016)). Also in these studies it is fundamental to well know the distance of central star which affects all the sizes characteristics of the circumstellar disk. This will allow us a proper comparison with theoretical models.

Acknowledgments

This project has received funding from the European Union's Horizon 2020 research and innovation programme under the Marie Sklodowska-Curie grant agreement No 664931. This work has made use of data from the European Space Agency (ESA) mission *Gaia* (`https://www.cosmos.esa.int/gaia`), processed by the *Gaia* Data Processing and Analysis Consortium (DPAC, `https://www.cosmos.esa.int/web/gaia/dpac/consortium`). Funding for the DPAC has been provided by national institutions, in particular the institutions participating in the *Gaia* Multilateral Agreement.

References

Andrews, S. M., Wilner, D. J., Zhu, Z., Birnstiel, T., Carpenter, J. M., *et al.* 2016, ApJL, 820, L40.
Armstrong, J. J., Wright, N. J., & Jeffries, R. D. 2018, MNRAS, 480, L121.
Bailer-Jones, C. A. L. 2015, PASP, 127, 994.
Brown, A. G. A., Arenou, F., van Leeuwen, F., Lindegren, L., & Luri, X. 1997, In *Hipparcos - Venice '97*, edited by R. M. Bonnet, E. Høg, P. L. Bernacca, L. Emiliani, A. Blaauw, C. Turon, J. Kovalevsky, L. Lindegren, H. Hassan, M. Bouf-

fard, B. Strim, D. Heger, M. A. C. Perryman, & L. Woltjer, *ESA Special Publication*, vol. 402, pp. 63–68.
Cantat-Gaudin, T., Mapelli, M., Balaguer-Núñez, L., Jordi, C., Sacco, G., *et al.* 2018, ArXiv e-prints.
Comerón, F., Reipurth, B., Henry, A., & Fernández, M. 2004, A&A, 417, 583.
Fedele, D., Carney, M., Hogerheijde, M. R., Walsh, C., Miotello, A., *et al.* 2017, A&A, 600, A72.
Fedele, D., Tazzari, M., Booth, R., Testi, L., Clarke, C. J., *et al.* 2018, A&A, 610, A24.
Feigelson, E. D. & Lawson, W. A. 2004, ApJ, 614, 267.
Franciosini, E., Sacco, G. G., Jeffries, R. D., Damiani, F., Roccatagliata, V., *et al.* 2018, A&A, 616, L12.
Gagné, J. & Faherty, J. K. 2018, ApJ, 862, 138.
Gagné, J., Faherty, J. K., & Mamajek, E. E. 2018, ApJ, 865, 136.
Gaia Collaboration, Brown, A. G. A., Vallenari, A., Prusti, T., de Bruijne, J. H. J., *et al.* 2018, ArXiv e-prints.
Haikala, L. K., Harju, J., Mattila, K., & Toriseva, M. 2005, A&A, 431, 149.
Haisch, K. E., Jr., Lada, E. A., & Lada, C. J. 2001, ApJL, 553, L153.
Hénault-Brunet, V., Gieles, M., Evans, C. J., Sana, H., Bastian, N., *et al.* 2012, A&A, 545, L1.
Hernández, J., Hartmann, L., Megeath, T., Gutermuth, R., Muzerolle, J., *et al.* 2007, ApJ, 662, 1067.
Jeffries, R. D., Jackson, R. J., Cottaar, M., Koposov, S. E., Lanzafame, A. C., *et al.* 2014, A&A, 563, A94.
Lindegren, L., Hernandez, J., Bombrun, A., Klioner, S., Bastian, U., *et al.* 2018, ArXiv e-prints.
Lindegren, L., Madsen, S., & Dravins, D. 2000, A&A, 356, 1119.
Luhman, K. L. 2007, ApJS, 173, 104.
Luri, X., Brown, A. G. A., Sarro, L. M., Arenou, F., Bailer-Jones, C. A. L., *et al.* 2018, ArXiv e-prints.
Mapelli, M. 2017, MNRAS, 467, 3255.
Pérez, L. M., Carpenter, J. M., Andrews, S. M., Ricci, L., Isella, A., *et al.* 2016, Science, 353, 1519.
Perryman, M. A. C., Lindegren, L., Kovalevsky, J., Hoeg, E., Bastian, U., *et al.* 1997, A&A, 323, L49.
Roccatagliata, V., Bouwman, J., Henning, T., Gennaro, M., Feigelson, E., *et al.* 2011, ApJ, 733, 113.
Roccatagliata, V., Sacco, G. G., Franciosini, E., & Randich, S. 2018, A&A, 617, L4.
Sacco, G. G., Spina, L., Randich, S., Palla, F., Parker, R. J., *et al.* 2017, Astronomy & Astrophysics, 601, A97. ISSN 1432-0746.
Sicilia-Aguilar, A., Hartmann, L., Calvet, N., Megeath, S. T., Muzerolle, J., *et al.* 2006, ApJ, 638, 897.
Stelzer, B., Micela, G., & Neuhäuser, R. 2004, A&A, 423, 1029.
Tognelli, E., Prada Moroni, P. G., & Degl'Innocenti, S. 2011, A&A, 533, A109.
van der Marel, N., van Dishoeck, E. F., Bruderer, S., Birnstiel, T., Pinilla, P., *et al.* 2013, Science, 340, 1199.
Voirin, J., Manara, C. F., & Prusti, T. 2018, A&A, 610, A64.
Whittet, D. C. B., Prusti, T., Franco, G. A. P., Gerakines, P. A., Kilkenny, D., *et al.* 1997, A&A, 327, 1194.
Zhang, K., Isella, A., Carpenter, J. M., & Blake, G. A. 2014, ApJ, 791, 42.